Surrogate-Assisted Prediction and Morphological Optimization of Dendritic Solidification Patterns

immediate

July 3, 2025

Abstract

1 Introduction

Dendritic growth, the formation of tree-like shapes, is a phenomenon that appears in several physical, biological, and engineering systems, including solidification processes [1], Li-ion deposition in batteries [2], synthesis of dendritic nanoparticles [3], and neuron growth [4]. Phase-field method (PFM) has become a cornerstone in modeling interfacial pattern formation, including dendritic growth, starting with solidification, which can be seen in a wide range of materials processes, from casting and additive manufacturing to battery electrode degradation [5, 6]. Phase field models effectively handle evolving boundaries without explicit tracking, eliminating a major computational bottleneck. However, they remain computationally expensive, requiring fine discretization and small time steps for accurate tip propagation and sidebranch resolution [7].

To overcome this limitation, data-driven surrogate models have emerged, enabling rapid prediction of microstructural evolution with high fidelity. Starting from basic statistical regressors [8], the field has progressed to convolutional and recurrent neural networks that can learn and predict phase-field dynamics, including dendritic growth, with significantly reduced computational cost [9]. A recent DeepONet surrogate further mimicked phase-field outputs in metal solidification [10], while other works have focused on reduced-order modeling via Gaussian processes and deep operators [11]. Still, most studies emphasize Cahn–Hilliard systems or isotropic grain growth, with few tackling fully anisotropic dendritic systems.

While prior work has explored deep learning for spatiotemporal prediction of dendritic solidification, such efforts have typically been limited in parametric diversity. For instance, Mao et al. [12] employed a ConvLSTM model trained on synthetic data generated using Kobayashi's phase-field model. Their dataset was constructed by varying the dimensionless latent heat parameter κ. However, a broader parametric variation would enable the surrogate to generalize over a wider range

of dendritic morphologies and support downstream tasks such as morphology classification and inverse design.

Furthermore, physics-informed neural networks (PINNs) have been shown to be capable of solving forward and inverse problems in PDE-governed systems by embedding physical laws into the training process [11, 13]. Phase Field-PINNs and domain-decomposed variants have been used to model solidification-like systems, including Cahn–Hilliard and Allen–Cahn equations, as well as fracture propagation and Navier–Stokes coupling [14]. However, applications of PINNs to spatiotemporal dendritic solidification with direct mapping from simulation parameters to evolving phase fields remain limited.

Beyond simulation, the challenge of characterizing the resulting morphologies remains critical. Scalar descriptors such as solid fraction, tortuosity, porosity, and the MacMullin number are widely used in fields like porous media [15] and batteries [16]. However, surrogate models rarely incorporate such metrics, let alone unify them into a dimensionless quantity that is interpretable, generalizable, and design-compatible.

In this paper, we develop both CNN-based and PINN-enhanced surrogates to directly map five-dimensional physical input parameters to full spatiotemporal phase-field outputs, $\xi(x, y, t)$. The training data is generated using an open-sourced FiPy-based numerical solver that models the coupled evolution of the phase field and temperature in 2D anisotropic solidification [17].

We further introduce ***dendricity***, D, a dimensionless morphological number that combines branching complexity (branchiness BR) and growth extent (solid fraction SF) into a single, interpretable metric. We show that D enables the classification of dendritic morphologies across regimes and can guide design via inverse mapping. Using our trained surrogate, we conduct optimization over the input space to target morphologies with specific dendricity ranges—demonstrating a powerful tool for accelerated, microstructure-aware materials design.

2 Problem Formulation

We consider the process of dendritic solidification governed by a two-field phase-field model that couples the evolution of a scalar order parameter $\xi(x, y, t)$ with the local undercooling field $\Delta T(x, y, t)$. The governing equations are given by:

$$\frac{\partial \Delta T}{\partial t} = D_T \nabla^2 \Delta T + \frac{\partial \xi}{\partial t}, \tag{1}$$

$$\tau \frac{\partial \xi}{\partial t} = \nabla \cdot (D \nabla \xi) + (\xi - 0.5) - \frac{\kappa_1}{\pi} \arctan(\kappa_2 \Delta T)(1 - \xi), \tag{2}$$

where τ is the relaxation time, D_T is the thermal diffusivity, and D is the anisotropic diffusivity tensor that depends on the orientation of the interface and the anisotropy strength c. The anisotropic tensor is expressed as:

$$D = \alpha^2(1 + c\beta) \begin{bmatrix} 1 + c\beta & -c\frac{\partial \beta}{\partial \psi} \\ c\frac{\partial \beta}{\partial \psi} & 1 + c\beta \end{bmatrix}. \tag{3}$$

where β encodes orientation-dependent anisotropy and ψ is the angle between the interface normal and the crystalline orientation.

The simulation is parameterized by a five-dimensional input vector:

$$\vec{p} = [\Delta T_0, c, N, \theta, r_0], \tag{4}$$

where: ΔT_0: initial undercooling, c: anisotropy strength, N: number of initial seed points, θ: crystal orientation angle, r_0: radius of the initial seed.

Given $\vec{p}$, the system evolves to produce a full spatiotemporal field $\xi(x, y, t)$ over a fixed computational domain and simulation time. The output of interest is a tensor of shape $\mathbb{R}^{N_x \times N_y \times N_t}$, representing the spatial and temporal evolution of the solidification morphology.

The central goal of this work is to construct a surrogate model F_θ that approximates the mapping:

$$F_\theta(\vec{x}) \approx \hat{\xi}(x, y, t), \tag{5}$$

where $\hat{\xi}$ is the surrogate-predicted morphology and θ denotes the trainable parameters of the model.

3 Surrogate Modeling Methodology

3.1 Data Generation

The training dataset was generated using a phase-field simulation framework implemented in Python through the open-source library FiPy [17]. The simulations are based on the two-field model introduced in Section 2, which couples the evolution of the order parameter $\xi(x, y, t)$ and the temperature field $\Delta T(x, y, t)$. The domain is a square computational grid of size $N_x \times N_y : 250 \times 250$ cells, and simulations are carried out for 750 time steps. The output fields are sampled every 25 steps, resulting in 30 stored frames per simulation.

Each simulation is fully defined by a five-dimensional input vector $\vec{p} = [\Delta T_0, c, N, \theta, r_0]$. For each simulation, the seed points are randomly distributed within the domain, and their radii are initialized uniformly using r_0. The boundary conditions are set to be Dirichlet for the temperature field and periodic for the phase field.

To construct a sufficiently diverse training set, we performed stratified sampling across a physically meaningful subset of the parameter space. The final dataset consists of 253 combinations spanning the following values for the inputs: Initial undercooling $\Delta T_0 \in \{-0.6,\ -0.4,\ -0.2\}$, anisotropy strength: $c \in \{0.005,\ 0.02,\ 0.05\}$, number of seed points: $N \in \{4,\ 6,\ 8\}$, orientation angle: $\theta \in \{0°,\ 15°,\ 30°,\ 45°\}$ initial seed radius: $r_0 \in \{0.08,\ 0.10,\ 0.15\}$.

The data set is divided into training sets 70%, validation sets 15%, and test sets 15%. This simulation data serves as ground truth for training the surrogate models described in the following

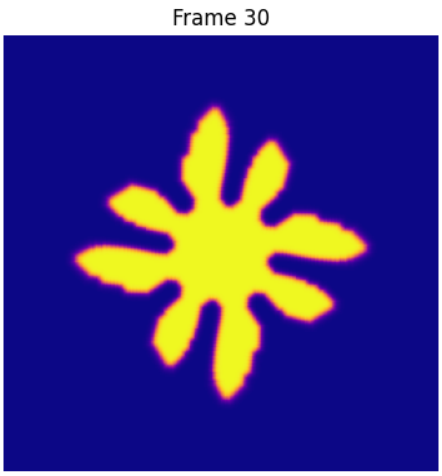

Figure 1: Sample dendritic morphology at the final simulation time step (frame 30) for input vector $\vec{p} = [\Delta T_0, c, N, \theta, r_0] = [-0.4, 0.005, 4, 15°, 0.1]$. The scalar field $\xi(x, y, t)$ represents the solidification order parameter, with yellow indicating solid ($\xi \approx 1$) and blue indicating liquid ($\xi \approx 0$).

sections.

3.2 Unified CNN–PINN Surrogate Architecture

To leverage the pattern-recognition power of convolutional neural networks (CNNs) while strictly enforcing the underlying phase-field PDEs, we propose a unified CNN–PINN hybrid. This model seamlessly integrates data-driven learning with physics-informed constraints.

3.2.1 Network Architecture:

Let $\mathbf{x} = \left[\Delta T_0,\ c,\ N,\ \theta,\ r_0\right]^{\mathsf{T}} \in \mathbb{R}^5$ be the input parameter vector. We first embed $\mathbf{x}$ via:

Subsequently, we apply L convolutional upsampling blocks:

$$h^{(l+1)} = \sigma\left(W^{(l)} * h^{(l)} + b^{(l)}\right),\ \text{for } l = 0, \ldots, L-1, \tag{6}$$

where $*$ denotes the convolution operator, $W^{(l)}$ and $b^{(l)}$ are the trainable kernel weights and biases at layer l, and $\sigma(\cdot)$ is the ReLU activation function.

$$\underset{\mathbb{R}^{5\times 1}}{\vec{p}} \xrightarrow{\textbf{CNN}} \underset{\mathbb{R}^{250\times 250\times 30}}{\hat{\xi}(t, \mathbf{x}, \mathbf{y})}$$

Physics-Informed Residual

We enforce the phase-field PDE residual:

$$\mathcal{R}_{i,j,t} = \tau \, \frac{\partial \hat{\xi}_{i,j,t}}{\partial t} \; - \; \nabla \cdot (D \, \nabla \hat{\xi})_{i,j,t} \; - \; \Big(\hat{\xi}_{i,j,t} - 0.5 - \tfrac{\kappa_1}{\pi} \arctan(\kappa_2 \, \hat{T}_{i,j,t}) \Big) \, (1 - \hat{\xi}_{i,j,t}), \tag{7}$$

where spatial derivatives use a five-point stencil,

$$\nabla^2 \hat{\xi}_{i,j,t} \approx \frac{\hat{\xi}_{i\pm1,j,t} + \hat{\xi}_{i,j\pm1,t} - 4\,\hat{\xi}_{i,j,t}}{\Delta x \Delta y},$$

and time derivatives use forward differences,

$$\frac{\partial \hat{\xi}_{i,j,t}}{\partial t} \approx \frac{\hat{\xi}_{i,j,t+1} - \hat{\xi}_{i,j,t}}{\Delta t}.$$

Composite Loss

The total loss blends data fidelity with PDE compliance:

$$\mathcal{L}_{\text{total}} = \lambda_{\text{data}} \underbrace{\frac{1}{N_{\text{b}} \, T} \sum_{b=1}^{N_{\text{b}}} \sum_{t=1}^{T} \big\| \hat{\xi}_t^{(b)} - \xi_t^{(b)} \big\|_2^2}_{\mathcal{L}_{\text{MSE}}} + \lambda_{\text{phys}} \underbrace{\frac{1}{N_{\text{b}} \, X \, T} \sum_{b,i,j,t} \mathcal{R}_{i,j,t}^2}_{\mathcal{L}_{\text{PDE}}}. \tag{8}$$

Here, N_{b} is batch size, $T = 30$ frames, and $X = 250^2$ spatial points. Hyperparameters λ_{data} and λ_{phys} are tuned on the validation set.

References

[1] A. Zaeem, M. H. Yin, and D. Felicelli, S.˙Modeling dendritic solidification of Al–3 % Cu using cellular automaton and phase-field methods. *Applied Mathematical Modelling*, 37(5):3495–3503, 2013.

[2] H. Lee, T. Kwak, W. Lee, J. Song, and D. Kim. Effect of surface topography on dendritic growth in lithium metal batteries. *Journal of Power Sources*, 552:232264, 2022.

[3] Yonghee Shin, Chiwon Lee, Myung-Seok Yang, Sunil Jeong, Dongchul Kim, and Taewook Kang. Two-dimensional hyper-branched gold nanoparticles synthesized on a two-dimensional oil/water interface. *Scientific Reports*, 4:6119, 2014.

[4] Kuanren Qian, Aishwarya Pawar, Ashlee S. Liao, Cosmin Anitescu, Victoria A. Webster-Wood, Adam W. Feinberg, Timon Rabczuk, and Yongjie Jessica Zhang. Modeling neuron growth using isogeometric collocation based phase field method. *Scientific Reports*, 12(1):8120, 2022.

[5] Ryo Kobayashi. Modeling and numerical simulations of dendritic crystal growth. *Physica D: Nonlinear Phenomena*, 63(3-4):410–423, 1993.

[6] Mohammad A Jaafar, Daniel R Rousse, Stephane Gibout, and Jean-Pierre Bédécarrats. A review of dendritic growth during solidification: Mathematical modeling and numerical simulations. *Renewable and Sustainable Energy Reviews*, 74:1064–1079, 2017.

[7] Tomohiro Takaki. Phase-field modeling and simulations of dendrite growth. *ISIJ international*, 54(2):437–444, 2014.

[8] Luca Parussini, Davide Venturi, Paris Perdikaris, and George Em Karniadakis. Multi-fidelity gaussian process regression for prediction of random fields. *Journal of Computational Physics*, 336:36–50, 2017.

[9] Zongyi Yang, Yiming Yin, Zhong Xu, Lei Liang, and Xiang Li. Microstructure evolution prediction via convolutional recurrent neural networks. *npj Computational Materials*, 8(1):78, 2022.

[10] David Ciesielski, Yichi Li, Shiyu Hu, Evan King, Jeffrey Corbey, and Panos Stinis. Deep operator network surrogate for phase-field modeling of metal grain growth during solidification. *Computational Materials Science*, 246:113417, 2025.

[11] Maziar Raissi, Paris Perdikaris, and George E Karniadakis. Physics-informed neural networks: A deep learning framework for solving forward and inverse problems involving nonlinear partial differential equations. *Journal of Computational Physics*, 378:686–707, 2019.

[12] Hong Mao, Chenyang Xie, Jingwen Pan, Qingzheng Cao, Xiaohong Zhang, Yun Luo, Yong Du, and Han Ning. Spatiotemporal prediction of solidified dendrites based on convolutional long-short-term neural network. *Materials Today Communications*, 41:110634, 2024.

[13] Nan Chen, Silvia Lucarini, Rui Ma, An Chen, and Chen Cui. Pf-pinns: Physics-informed neural networks for solving coupled allen–cahn and cahn–hilliard phase field equations. *Journal of Computational Physics*, page 113843, 2025.

[14] Shreyas Kathane and Shanthanu Karagadde. Domain decomposition physics-informed neural networks (dd-pinns) for modeling alloy solidification with moving boundaries. *Computational Materials Science*, 232:112144, 2024.

[15] Stephen Ryan, Samuel Cooper, Dan J L Brett, and Paul R Shearing. Quantifying the tortuosity of porous media from embedded simulation domains. *Transport in Porous Media*, 138:107–126, 2021.

[16] Chien-Hsun Chen and Chun-Wei Pao. Phase-field study of dendritic morphology in lithium metal batteries. *Journal of Power Sources*, 484:229203, 2021.

[17] examples.phase.anisotropy — fipy 3.4.4 documentation. `https://www.ctcms.nist.gov/fipy/examples/phase/generated/examples.phase.anisotropy.html`. Accessed: 2025-03-21.